Guided Entry: A Necessary Step from Exomars to Precision Landing on Mars

M. Buonocore(*), J. Ospina(**), E. Canuto(**), A. Bacchetta(*), F. Calantropio(*), A. Martelli(*), D. Oddenino(*)
(*) Thales Alenia Space Italia, Strada Antica di Collegno, 253 - 10146 Torino (Italy),
email: marcello.buonocore@thalesaleniaspace.com
(**) Politecnico di Torino, Dip. di Automatica e Informatica, Corso Duca degli Abruzzi 24, 10129 Torino
email: jose.ospina@polito.it

Abstract

Thales Alenia Space Italia is currently involved in the development of GNC technologies for Mars Entry, Descent and Landing (EDL) system within two ESA projects: the EXOMARS "EDM", to provide Europe with soft landing capability on a 75 km landing ellipse, and MSR related studies, with a 10 km required landing ellipse. A Guided Entry phase of a lifted capsule is mandatory for facing this challenge. This paper describes the principles that drove the design of a GNC algorithm able to control it during the different flight regimes of the entry phase up to the parachute deployment point and some preliminary promising results of its performance and robustness.

1. Introduction

Thales Alenia Space Italia (TAS-I) is currently involved in the development of Guidance, Navigation and Control (GNC) technologies for Mars Entry, Descent and Landing (EDL) system within two projects of the European Space Agency.

1) The ESA-NASA ExoMars (EXM) programme with TAS-I as prime contractor. The 2016 mission scenario includes a Mars Orbiter and an Entry, Descent and Landing Demonstrator Module (EDM). The latter will provide Europe with soft landing capability on the surface of Mars with a required downrange semi-major axis of the landing ellipse better than 75 km (3-sigma, TBC), [1].

2) Mars Sample Return (MSR) Phase A2 system definition studies led by TAS-I, with a required downrange semi-major axis of the landing ellipse better than 10a km (3-sigma). In contrast to the spin stabilized entry of the ExoMars EDM, a guided entry is mandatory for achieving the MSR challenging landing accuracy requirement. A small Center of Gravity (CoG) offset is created to generate a non-zero lift, which vertical and horizontal components are modulated by acting on the aerodynamic bank angle; a guidance law that controls this lift vector through banking manoeuvres corrects for down-track and cross-track errors. Such a solution has been adopted for the NASA Mars Science Laboratory mission that aims to deliver a rover within a ~20 km landing circular region [2].

In addition, a collaborative research project is on-going between Thales Alenia Space and Politecnico di Torino. The project has the main objective to study and develop control algorithm(s) for the guided entry of a lifted capsule in the Martian atmosphere. The candidate algorithm will operate during the different flight regimes of the entry phase, from atmospheric Entry Interface Point (EIP) up to the Parachute Deployment Point (PDP).

According to Kluever [3], two different approaches can be identified for the design of the guided entry algorithm: reference path tracking and predictive path-planning methods. A large heritage of the Apollo guided entry algorithms is still used as the basis for reference path tracking algorithms. In fact, flight-tested algorithms of the Atmospheric Reentry Demonstrator of ESA [4] and about-to-flight algorithms of Mars Science Laboratory from NASA [5], uses an Apollo-derived control scheme. On the other side, some interest has been recently focused on the development of path-planning algorithms such as those proposed by Tu [6] Bayard [7] , and, more recently, by Lafontaine [8].

Here, a rather midway approach is chosen. The analysis is performed using a model based technique which follows the principles of the Embedded Model Control (EMC) methodology, developed at Politecnico di Torino (see [9] for a theoretical overview and [10], [11], [12], [13] and [14] for a recent applications on aerospace control). The proposed solution tackles the problem of dispersion at the parachute deployment point by dealing with each of its causes separately:

1) Entry point (EIP) state dispersion: a reference trajectory (and bank angle profile) is recalculated at the EIP such that initial errors are compensated and the final full state (velocity, flight path angle, heading, altitude, lateral and longitudinal) at the PDP is obtained, taking into account the bank reversals maneuvers. This is a path-planning algorithm but is computed only once, at EIP.

2) Atmospheric and aerodynamic dispersions: the effect of the atmospheric and aerodynamic dispersion on the capsule motion is estimated in real time using a model of the longitudinal dynamics. Once known, the effect of these dispersions is directly compensated by adjusting the bank angle. The core of the technique relies on the extraction of the disturbance signals from the combination of the measurements and the model.

As it will be shown below, using the model-based methodology of the EMC allows for the control algorithm to compensate each cause of dispersion such that the resulting dispersion at the PDP is significantly smaller than the one claimed by other reference path tracking and predictive path approaches (see dispersion plots on [5] and [8]).

The guided entry algorithm is designed independently from the nominal entry considerations and then a nominal entry profile is here assumed available to the GNC at the Entry phase start. On the other end, the generation of a nominal entry profile is out of the scope of the present paper: some analyses about how an optimal nominal trajectory could be obtained are treated in [21], [22] and [23].

To fully characterise a nominal profile is enough to provide the nominal EIP conditions and the nominal bank angle profile. In fact, as mentioned above, the path-planning logic, implemented here, is not aimed at requirements verification but simply at recovering the EIP dispersion. The following considerations support such an assumption:

1) The entry corridor is thin; therefore, there is a limited freedom to flight along paths different from the nominal one in order to respect the capsule requirements (load factor, heat flux, etc.).

2) The controllability of the capsule position is limited. In fact, using the command to keep the capsule around a nominal trajectory already results in command saturation due to aerodynamic and atmospheric dispersion. Asking guided entry to reduce dispersion and also to avoid dangerous trajectories from generic entry conditions seems unfeasible for biconic low L/D entry capsules.

The performance and robustness of the candidate guided entry algorithm(s) has been already verified on a realistic 6DOF simulator. It performance will be consolidated on an EXOMARS Descent Module derived end-to-end simulator that will be enhanced during the research activity. In order to use a realistic verification test bed, the applicable scenario will be the MSR one as consolidated during TAS-I during Phase A2 studies.

Before entering into the details of the guided entry algorithms, an overview of the ballistic scenario, based on EXOMARS mission is included, showing the reasons for which lifted trajectories becomes necessary for future mission concepts.

1.1. EXOMARS EDM Ballistic Entry

The main objectives of the 600 Kg EDL Demonstrator Module (EDM) are to demonstrate European capability to land on Mars and to validate EDL system technologies with growth potential and suitable for delivering different science surface payloads. The GNC plays the fundamental role to achieve the safe Entry, Descent and Landing, in particular to reconstruct the EDM attitude after exiting from hibernation before entry, to determine the triggers enabling the various modes of the EDM mission and to command the thrusters during landing. Only the landing is a controlled phase, where the classic g-turn strategy is adapted to implement also a fast avoidance maneuver of the EDM separated items. Predictable touchdown conditions of the landed platform are mandatory to avoid overturn, so permitting correct data-transmission to the Orbiter [15]. The lacking of a precision landing requirement drives the landing footprint to a size comparable with the one observed in the NASA's MER mission. According to a dispersion sensitivity analysis made for MER [16] and shown in Figure 1, the main contributor to the landing dispersions is the atmosphere knowledge uncertainty, while other significant contribution arises from the aerodynamic coefficient knowledge: all these quoted factors contributes to a final 99% landing ellipse (2D normal distribution 3 ellipse) of more than 60 km (major axis)

An effective entry phase is able to decelerate the capsule reaching safe conditions for the parachute opening. Entry system's deceleration and heating profile are governed by EIP conditions and the hypersonic ballistic coefficient β, which is given by its mass m, drag coefficient c_D, and reference area S_{ref} as $\beta = m/c_D S_{ref}$. The time the velocity is low enough to deploy supersonic or subsonic decelerators, the vehicle may be near the ground with insufficient time to prepare for landing, especially for high landing Mars elevation (> 0 km MOLA, Mars Orbiter Laser Altimeter

topography) as targeted by future missions. Mars' low atmosphere density coupled with deceleration requirements has led to entry systems, like the Viking heritage 70-degree sphere cone, designed to produce a high hypersonic drag coefficient (i.e. theoretically $c_D \approx 1.7$ at zero angle-of-attack).

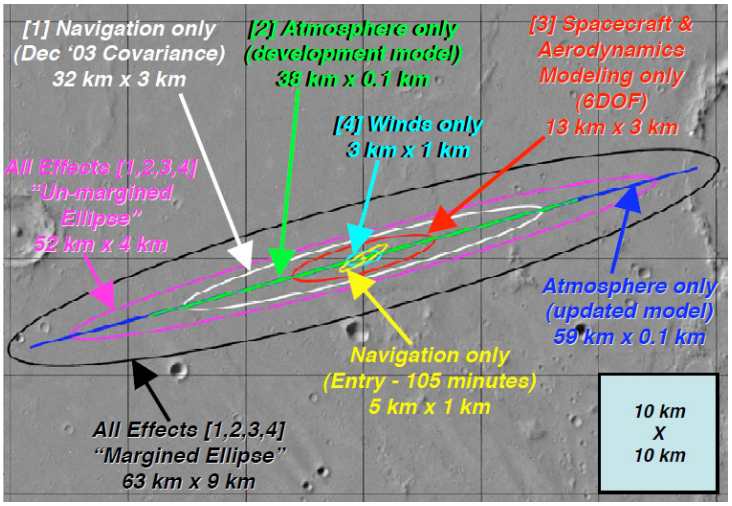

Figure 1. Contributors to MER Landing Dispersions, [16]. Reprinted with permission of the American Institute of Aeronautics and Astronautics.

To the date the ballistic coefficient has ranged from 63 to 94 $\mathrm{kg/m^2}$: since the latter is a significant driver on the parachute deployment altitude and the subsequent EDL events timeline, as landed mass is increased, the aero-shell diameter must also increase, reaching 4.5 m for the next US mission Mars Science Laboratory (MSL) to be launched by the end of this year, with a parallel increase of the β to 115 $\mathrm{kg/m^2}$ for accommodating a 2800 kg entry mass, [17] [18]. As a 4.5 m diameter should be an upper limit in the current launch capabilities, mass increase will lead to higher β and lower PDP altitudes: using the extraordinarily-high packaged density of the MER aeroshell as an upper-limit and noting that to first-order, β increases linearly with diameter, the maximum β for a 4.5 diameter 70-deg sphere cone is approximately 153 $\mathrm{kg/m^2}$, the largest β one can imagine for robotic Mars systems over the next several decades, [17]. Entry corridor for such higher β may by empty or may miss the Q-box for safe parachute deployment. A remedy for this problems consists in adding lifting capabilities to the capsule (aerodynamic lifting of the order of L/D=0.22) with the further advantage of allowing a guided entry by controlling the lift direction. Refer to [17] to visualize how the entry altitude for different ballistic coefficients increases in case of lifted entry. Figure below shows the altitude increase of the entry altitude for different ballistic coefficients in case of lifted entry.

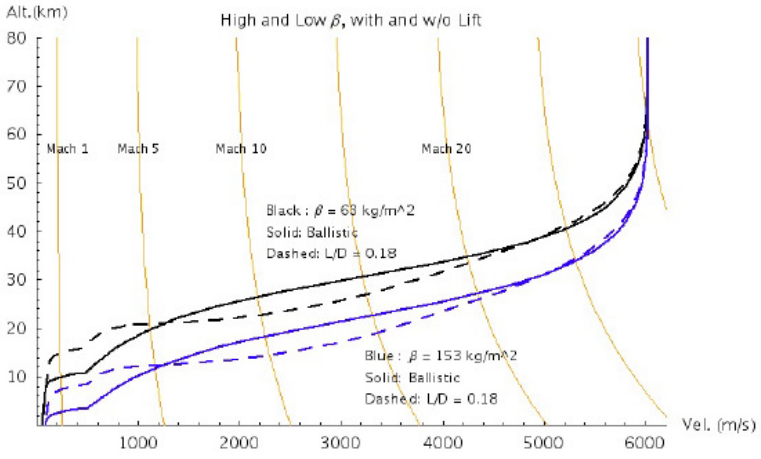

Figure 2. Ballistic and lifting (vertical L/D = 0.18) Mars EDL nominal trajectories for β = 63 and 153 kg/m2, [17] (© 2006 IEEE)

2. Mars Sample Return Scenario

2.1. Mission architecture

The ESA's Mars Robotic Exploration Program (MREP) is intended to prepare Europe's future contribution to the international exploration of Mars, [19]. Mars Sample Return (MSR) mission is taken as MREP long term objective and is a fundamental step to validate technologies and operations needed for future human exploration at reduced scale. Scientific objectives of MSR would ask for both precision landing and high ballistic coefficient.

The proposed MSR would be a campaign of three segments:

1) a sample caching mission, which would cache rock cores for later pickup,
2) the MSR Lander Mission, which would retrieve the sample and place it in Mars orbit in the form of a container called the orbiting sample (OS), and
3) the MSR Orbiter Mission, which would return the OS to the Earth's surface.

A fourth component is the Mars Returned Sample Handling (MRSH) element that would include a sample receiving facility (SRF).

The mission segment #2, and in particular the lander carrying the Mars Ascent Vehicle (MAV) is the objective of the present paper: after separation by its carrier, a Descent Module (DM) will precisely land the MAV, used for Mars surface operations and to deliver the collected terrain to the Earth Re-entry Capsule (ERC).

The entry mass of the DM is 2200Kg and due to its dimensions, provided below, the entry will cope with a ballistic coefficient close to 100 kg/m^2 .

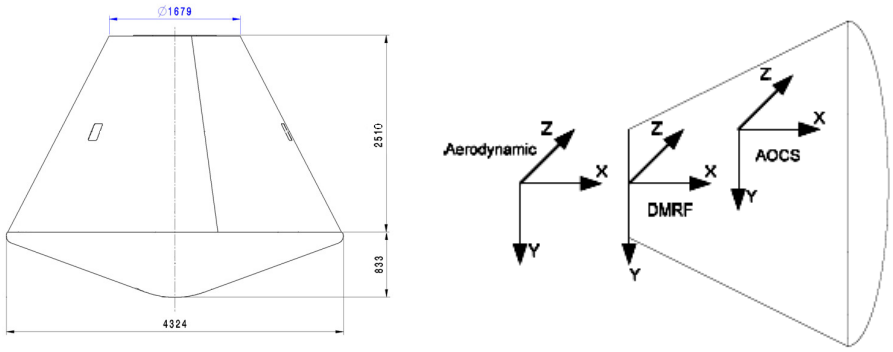

Figure 3. MSR DM Dimensions (Left) and Reference Frames (Right: AOCS Frame is centered in the CoG, offset at [1.4, -0.101, 0] meters wrt the DM Reference Frame)

The 10 cm offset shown in the figure above is able to trim a total angle of attack of around 17 deg, leading the capsule to flight in the Mars atmosphere with a L/D ratio of 0.25.

2.2. Unguided Lifted Entry

A preliminary Montecarlo simulation using a 3DOF entry simulator is computed to assess an error budget of the PDP dispersion due to different causes: position and velocity dispersion at EIP and uncertainty on the aerodynamic database and the atmospheric density. The PDP is chosen based on an altitude triggering schema. A table summarizing the nominal EIP and bank angle profile is included in Table 1. The EIP Flight Path Angle (FPA) is increased (in the steeper sense) to -15 deg to cope with the current scenario for similar missions. The dispersion assumptions for the Montecarlo simulation are shown in Table 2.

Being a 3DOF simulation, aerodynamic coefficients are only the lift and the drag ones, whose dispersion is actually obtained from the combination of the axial and normal coefficients and the Center of Mass (CoM) offset, using a procedure that is not included here. Table 2 shows their standard deviation. Lift and drag coefficients dispersions are actually correlated and this is also considered for the Montecarlo simulation. All distributions are assumed uniform and the PDP is chosen based on an altitude based triggering algorithm.

Table 1. Nominal entry conditions		
Variable	**3 σ**	**Units**
Altitude	120 km	km
Longitude	-9	deg
Latitude	21.5	deg
Velocity	5560	m/s
Fligth path angle	-15	deg
Heading	132	deg
Constant bank angle cosine	0.5	-
CoM Offset	0.1	m

Table 2. Dispersion assumption for Montecarlo simulations					
Variable	**3 σ**	**Units**	**Variable**	**3 σ**	**Units**
Along track position	5	km	Axial coeff.	10	%
Cross track position	5	km	Normal coeff.	10	%
Radial position	5	km	CoM position	5	mm
Along track velocity	10	m/s	Density	3 × EMCD dispersion	
Cross track velocity	25	m/s	Drag coeff.	8	%
Radial velocity	15	m/s	Lift coeff.	25	%

Different Montecarlo simulations are computed by considering each source of dispersion separately. The resulting error budget of the PDP dispersion is summarized in Table 3 and depicted in figure below:

Table 3. PDP horizontal dispersion budget		
Variable	**Semi major axis [km]**	**Semi minor axis [km]**
Velocity at EIP	25	5
Position at EIP	70	10
CoM state at EIP	71	11
Drag and Lift coeff.	100	0
Atmospheric density	20	0
All effects combined	130	25

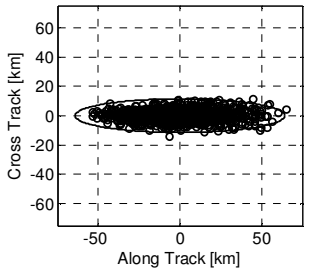

Figure 4. Landing Dispersion as result of the contributions listed in Table 3

3. Mars Sample Return Guided Lifted Entry

Following the principles of the Embedded Model Control, and based on the results of the preliminary dispersion analysis, the following structure for the design of the Guided Entry GNC algorithms is considered:

1) The dispersion at the EIP is tackled by a guidance algorithm which finds a bank angle profile that will make the capsule to reach the nominal PDP starting from the navigated EIP. This is achieved separating the longitudinal and the lateral motion and by iteratively solving optimal point-to-point control problems based on a linearized dynamics around the guidance trajectory.

2) Atmospheric and environmental dispersion are seen as external disturbances. A "tracking" CoM control to compensate disturbances and keep the capsule state locked around the guidance trajectory. This is achieved using an extended state observer combined with an active disturbance cancellation control law.

3) The attitude control is considered the "actuator" of the CoM control algorithms, since it keeps the bank angle of the capsule at the required value. The attitude control is designed around a simplified attitude dynamics which put in evidence the different relation between commanded torque and aerodynamic angles.

To perform the GNC task, the capsule would rely on a three axis Inertial Measurement Unit (IMU) (including gyros and accelerometers) and a Pulse Width Modulated (PWM) Reaction Control System (RCS) able to command,

as a baseline, up to ~300 Nm control torques along roll axis, while leaving sufficient manoeuvrability to pitch (~30 Nm) and yaw (~100 Nm) axes.

Most of the analysis done until the date has been focused on the guidance and control problem, leaving the navigation problem as a typical IMU strap-down scheme with, eventually, relying on the Drag Derived Altitude (DDA) capabilities [4]. It is expected that navigation errors will not degrade the performance of the guidance and control algorithms but that will simply combine to them as an independent dispersion source, coherently with the results obtained by Kluever [3].

In the following sections, the guidance and control algorithms are explained in more detail together with an overview of the attitude control algorithm.

3.1. Overview of the CoM Guidance

The guidance algorithm scope is to find a bank angle profile that is able to drive the CoM position and velocity to the desired mission PDP state from the navigate state at EIP. Note that the PDP state refers to three position and three velocity components. In practice it does this based a set of non-linear differential equations describing the entry motion for a round rotating planet

$$\dot{r} = v \sin\gamma S \qquad \dot{v} = -\frac{F_D}{m} - g\,\mathrm{s}_\gamma + r\omega_M^2\,\mathrm{c}_\lambda\left(\mathrm{s}_\gamma \mathrm{c}_\lambda - \mathrm{s}_\lambda \mathrm{c}_\chi \mathrm{c}_\gamma\right)$$

$$\dot{\Lambda} = \frac{v\cos\gamma\sin\chi}{r\cos\lambda}\text{, and } \dot{\gamma} = \frac{F_L}{mv}c_\mu + \left(\frac{v}{r} - \frac{g}{v}\right)\mathrm{c}_\gamma + 2\omega_M\,\mathrm{s}_\chi \mathrm{c}_\lambda + \frac{1}{v} r\omega_M^2\,\mathrm{c}_\lambda\left(\mathrm{c}_\gamma \mathrm{c}_\lambda + \mathrm{s}_\lambda \mathrm{c}_\chi \mathrm{s}_\gamma\right) \tag{1}$$

$$\dot{\lambda} = \frac{v\cos\gamma\cos\chi}{r} \qquad \dot{\chi} = \frac{v}{r}\mathrm{c}_\gamma \mathrm{s}_\chi \mathrm{t}_\lambda + \frac{\mathrm{s}_\mu F_L}{v\,\mathrm{c}_\gamma} + 2\omega_M\,\mathrm{s}_\lambda - \mathrm{c}_\chi \mathrm{c}_\lambda\, t_\gamma + r\omega_M^2\,\frac{\mathrm{s}_\chi \mathrm{c}_\lambda \mathrm{s}_\lambda}{v\,\mathrm{c}_\gamma}$$

where the trigonometric functions are simplified in notation as $c_x = \cos x$, $s_x = \sin x$ and $t_x = \tan x$, x being a generic angle. In (1), r is the distance to the center of the planet, Λ is the longitude, λ is the latitude, v is the modulus of the co-rotating velocity, γ is the FpAand χ is the heading angle. The mass m, the gravity g and the planet angular rotation ω_M are considered constant parameters while the drag and lift forces are expressed as

$$\begin{aligned} F_D &= S_{ref} c_D \frac{1}{2}\rho v^2 \\ F_L &= S_{ref} c_L \frac{1}{2}\rho v^2 \end{aligned} \tag{2}$$

It is assumed, as a condition, that the nominal bank profile includes a certain number of Bank Reversal Manouvers (BRM) in which the sine of the bank angle is sign toggled while its cosine is kept constant. This assumption allows for the separation of the dynamics into the longitudinal and lateral motion, which largely simplifies its analysis.

The scope of the guidance algorithm is then to adjust the profile of the bank angle with respect to the mission profile such that the dispersion (the one that can be estimated by the navigation) at the EIP is recovered. The principles over which the guidance algorithm is designed are:

1) The set of equations are separated into two independent sub sets: The longitudinal dynamics and the lateral dynamics.
2) Based on the longitudinal set of equations, the nominal time elapsed from the EIP to the PDP is adjusted. It is done by trying to optimize (reduce) the size (L-inf norm) of the bank angle deviations that the longitudinal guidance algorithm will compute. This is achieved by using an optimal time search algorithm that is based on a gradient descent search algorithm which, in turn, uses a simplified 2DOF (longitudinal) set of equations.
3) Based on the 3DOF set of equations and the results of the optimal time search algorithm the vertical component of the lift, denoted as u_γ is adjusted such that the PDP longitudinal state is reached. (downrange, altitude, velocity modulus and flight path angle).

4) Based on the 3DOF set of equations, the time instants in which the BRMs are commanded are adjusted such that the PDP lateral state is reached.

5) An iterative procedure couples the solution of the longitudinal and the lateral algorithms and builds a compatible bank angle profile.

6) The resulting bank profile has a bounded (and programmable) maximum second derivative, which is selected based on the maximum torque of the thrusters.

The result of each of the steps mentioned above is shown in the figures below.

Left side on Figure 5 shows different intermediate solutions of u_γ that is able to recover EIP dispersion based on a 2DOF set of equations. The only difference between one solution and the other is that the final time is slightly adjusted. As it cab be seen, the L-inf (maximum value of the absolute value) of each solution changes with the final time until it reaches a minimum value. For the case shown in the figure, the L-inf norm passes from 1.1 to 0.8 by extending the entry phase duration of 25 seconds. Note that, being a cosine, values larger than 1 are impossible.

Right side of Figure 5 shows the distribution of the output of the optimal time search algorithm for several different EIP dispersion extracted according to Table 2.

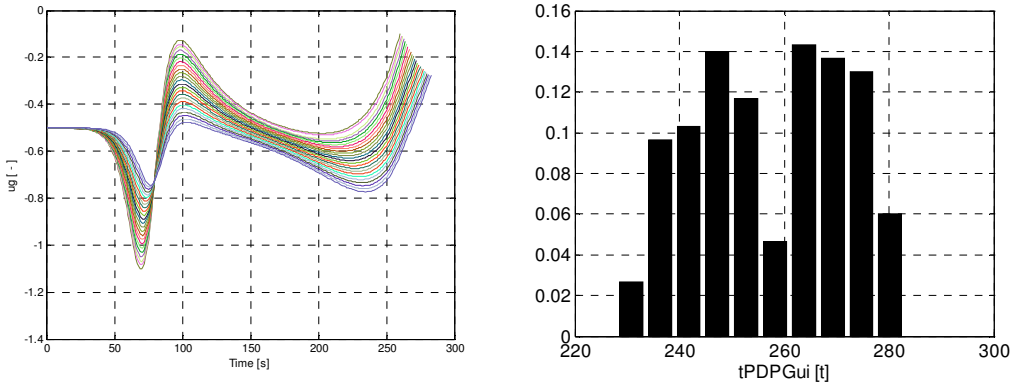

Figure 5. Different solutions for u_γ computed by the simplified 2DOF longitudinal guidance for different selection of the final time.

In Figure 6, the output of the solution of the longitudinal guidance is shown. As it can be seen, even in the presence of a 4 km radial error at EIP, the four components of the longitudinal state can reach the nominal PDP. Three trajectories are shown: the mission nominal, the trajectory in which the mission bank angle profile is kept, and the longitudinal guidance trajectory.

In Figure 7, the output of the lateral guidance is shown. It shows a 4 BRMs entry profile with constant cosine of bank angle. The instants at which each BRM is commanded are adjusted iteratively to reduce the lateral error at PDP. On the left figure, the evolution of the crossrange shows how the algorithm reaches the lateral state at PDP after the second iteration. "Nom" refers to the nominal mission trajectory, NC is the trajectory without guidance (keeping the nominal bank profile) and the different iterations show the crossrange evolution for each step of the iterative algorithm.

Several different bank angle profiles, obtained as the output of the iteration of the longitudinal and lateral algorithms are shown in Figure 8. On the right side, a plot of the distribution of the entry phase duration (from EIP to PDP) is included. As it can be seen, bank angle profiles and final time have relevant variations even though the dispersion at EIP to be recovered is only 5 km. This is probably a result of the low controllability of the capsule.

The dispersion of the final PDP state obtained using the profiles shown in Figure 8, for and EIP (known) dispersion of 5 km, is shown in Figure 9. Notice that the dispersion of the guidance algorithm can be reduced by increasing the number of iterations. Currently, 5 iterations are computed taking, on a Intel® Core™ i5 CPU M520 @ 2.40 GHz, about 2-3 seconds of computing time.

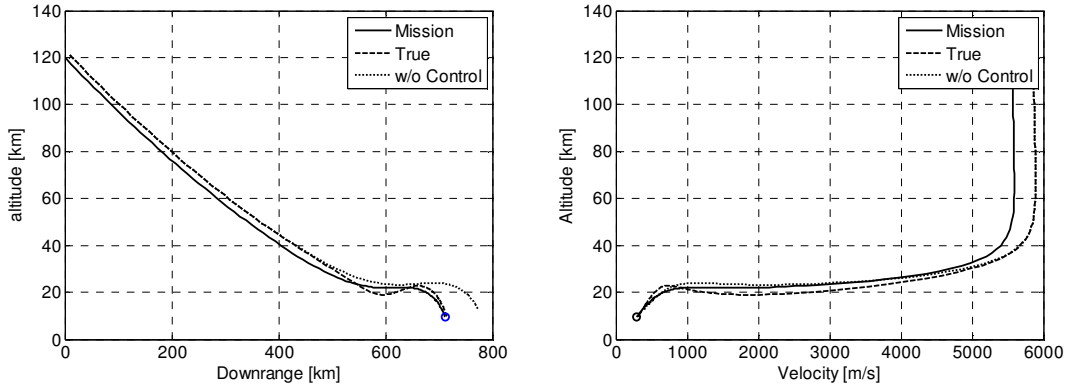

Figure 6. Longitudinal guidance algorithm. Recovering, in this case, 4 km on EIP altitude error.

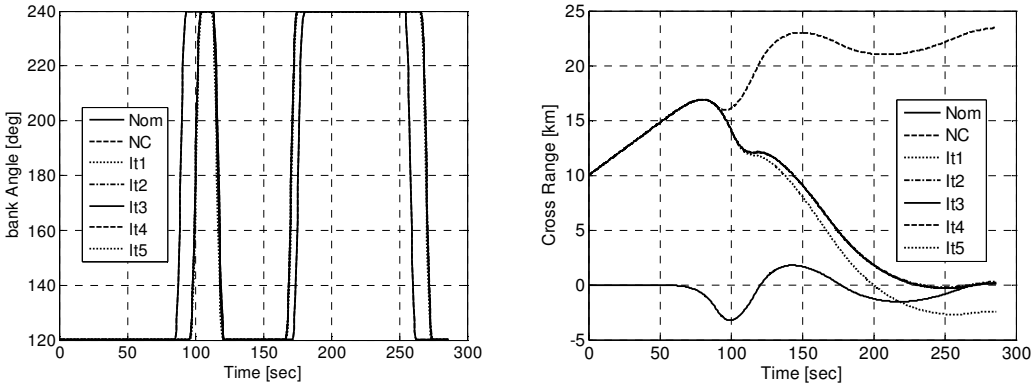

Figure 7. Lateral guidance algorithm. (LEFT) Evolution of the bank angle profile after different iterations. (RIGHT). Crosstrack showing a recovery of 10 km and 1 deg of heading errors at the EIP.

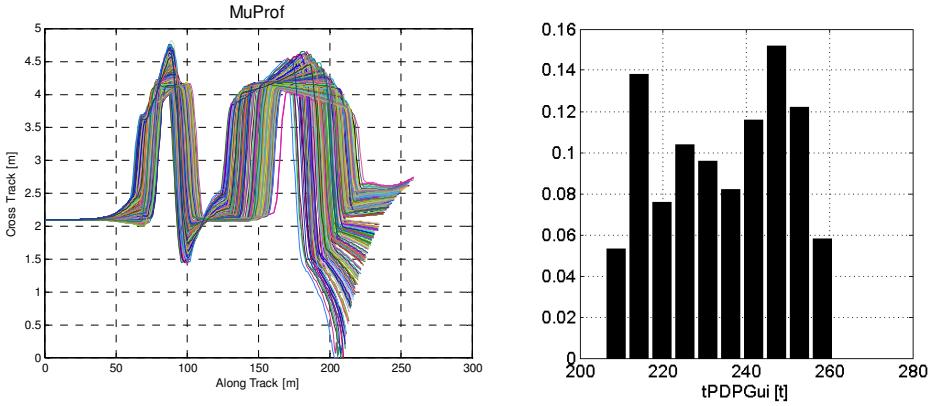

Figure 8. (LEFT) Superposition of the bank reversal profiles calculated by the guidance. (RIGTH) Distribution of the output of the optimal time search algorithm.

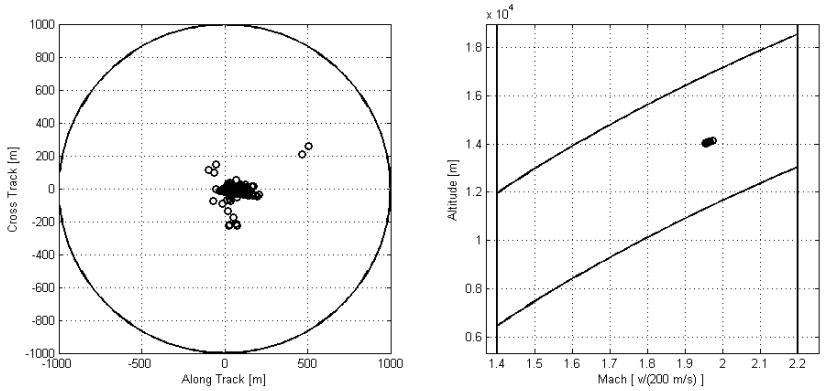

Figure 9. PDP horizontal and altitude-velocity dispersion of the guidance algorithm. Circle denotes 1 km.

3.2. CoM Control

Once the guidance trajectory has been obtained, a tracking control algorithm is designed to keep the trajectory of the capsule locked to it, even in the presence of aerodynamic and atmospheric dispersion (wrt to the nominal profiles used by the guidance computation). The work-load of the tracking algorithm is drastically relaxed by the guidance algorithm, since it offers, as output, a "natural trajectory ", i.e. it respects equations (1) and ask for a bank angle profile with bounded second derivative.

Deviations from the guidance trajectory will be caused by the error of the nominal aerodynamic (c_L and c_D) and atmospheric (ρ) conditions. The tracking algorithm needs, then, to compensate for these causes by adjusting the bank angle profile during the entry phase. This is achieved by following a similar principle as the one used for the guidance algorithm, i.e., the longitudinal and lateral dynamics are treated separately.

The longitudinal dispersion is compensated based on the linearization of the longitudinal dynamics around the guidance trajectory. This linearization, expressed as a time-varying linear set of discrete state equations, is extended to include the real time estimation of the dispersion causes (disturbances) and referred, under the EMC methodology, as the "embedded model". The structure of the longitudinal embedded model is shown in Figure 10.

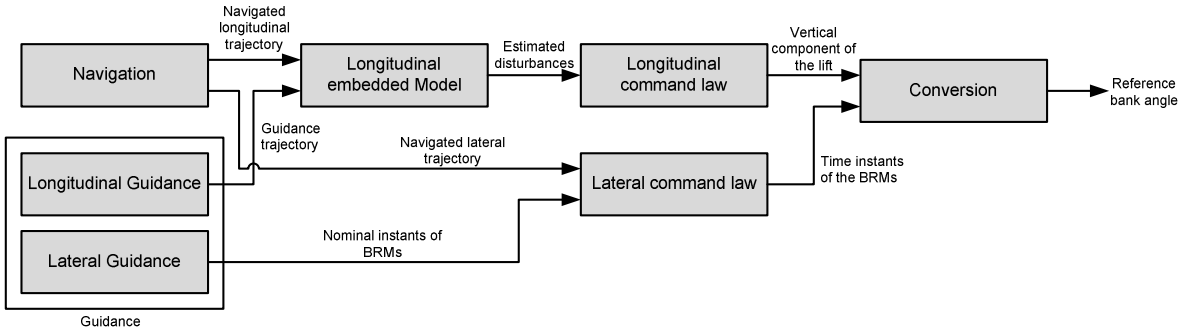

Figure 10. Structure of the CoM control algorithm.

The structure on Figure 11 is used to estimate the disturbance signals, one affecting as lift does, and the other as drag. The command (in this case the variations on the vertical component of the lift) is adjusted to counteract the effect of these causes. The law that is used to calculate this command is described in [9], it is the core of the EMC methodology and is based on the internal model principle of the linear regulator theory, which states that, in order to cancel an external disturbance, it is necessary to include a model of it inside the control unit.

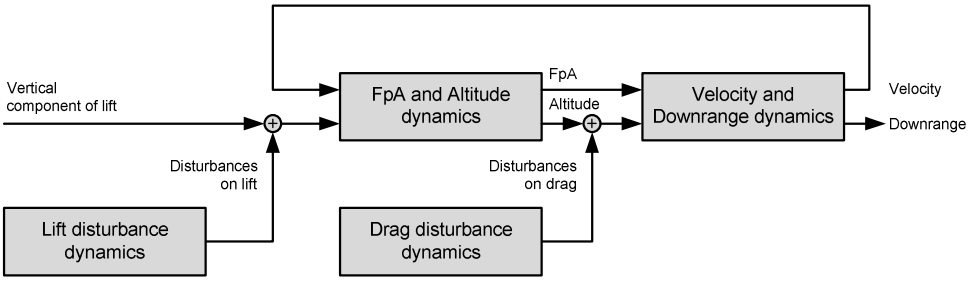

Figure 11. Structure of the longitudinal embedded model

The solution of the command law actually depends on the parameters of the longitudinal dynamics, which are time-varying, and are extracted from guidance trajectory. The approach that has been followed is a gain-scheduling algorithm in which the close loop poles are kept fixed.

A typical evolution of the longitudinal control law is shown in Figure 12. In this case the mean error on the drag coefficient is -5 %, on the lift coefficient is -10 % and on the density is 20 %. It can be seen that the bank angle is able to compensate the deviations on the downrange error (ds on the figure), keeping it bounded and below 2 km.

The longitudinal embedded model describes the relationship between the deviations of the longitudinal state variables (FPA, altitude, velocity and downrange) wrt to their guidance profiles. It puts into evidence that, in order to reduce the downrange dispersion, it is necessary to reduce also the dispersion on the FPA, altitude and velocity. In other words, the embedded model says that, in order to regulate the downrange, it is mandatory to regulate also the flight path angle, the altitude and the velocity modulus.

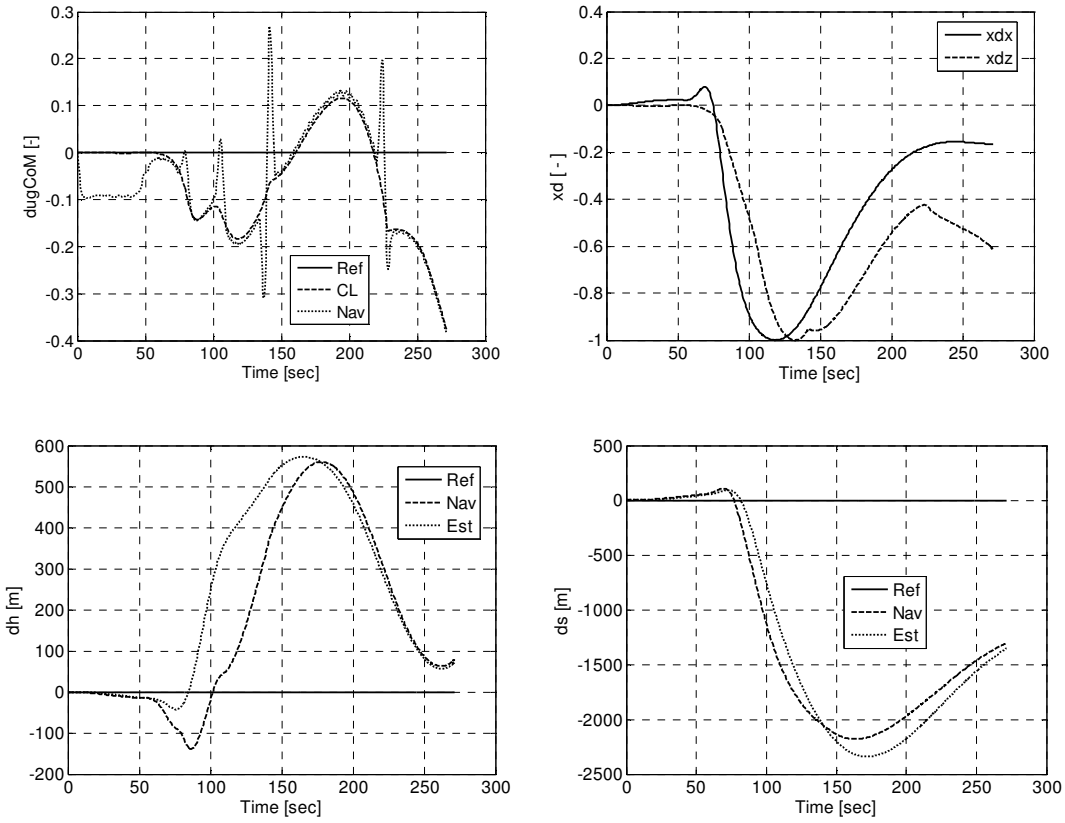

Figure 12. (TOP) Evolution of the longitudinal command Δu_γ and the estimated disturbances (scaled). (BOTTOM) Evolution of the altitude and down-rage deviation of the capsule trajectory.

3.3. Attitude control

The scope of the attitude control is twofold: to drive the bank angle along a reference trajectory, obtained as the combination of the guidance algorithm and the current request of the CoM control algorithm and to damp the aerodynamic angles (total angle of attack and aerodynamic roll) around their natural equilibrium.

The aerodynamic angles used here are defined as the 1-2-1 sequence of rotations from the velocity reference frame to the body reference frame. The first rotation is the aerodynamic bank angle (refer in this document as bank angle), the second the total angle of attack and the third one is the aerodynamic roll. This definition is assumed instead of the typical 1-3-2 rotation of "geometrical bank angle", (inverted sign) sideslip and angle of attack, in which the geometrical bank angle would differ from the aerodynamic bank angle.

The command of the attitude control is considered a bipolar signal ON/OFF to be sent to the thrusters, which are considered pulsed thrusters according to the MSR scenario. Actually, the control algorithm computes the commanded torques, which are then converted into the propulsion requested to each thruster (in [N]) and subsequently converted into the duty cycle of the ON/OFF signal.

The design of the attitude control follows, again, the principles of the EMC methodology. It is based on a simplified set of set of state equations which describes the aerodynamic angles dynamics, considering as inputs the three components of the thrusters torque and the time-derivative of the velocity angles (FPA and heading). This set of equations would correspond to the attitude embedded model.

The attitude embedded model is obtained by handling, transforming and simplifying the aerodynamic angles dynamics. The resulting structure is shown in Figure 13.

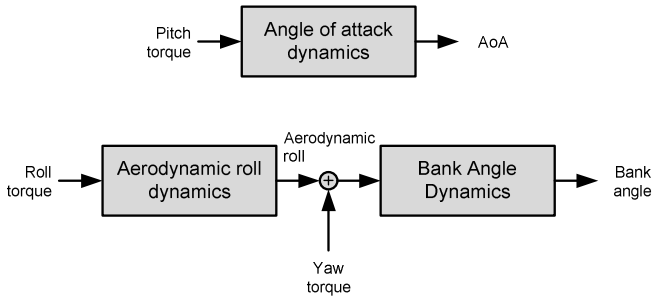

Figure 13. Structure of the attitude dynamics embedded model

The main concepts that can be extracted from Figure 13 which represents the baselines for the design of the control unit, are:

1) The AoA dynamics are uncoupled from those of the bank angle and the aerodynamic roll.
2) The bank angle is actually commanded by the yaw torque, while the roll torque is necessary only to keep the aerodynamic roll around its equilibrium.
3) Although bank angle dynamics is of fourth order, it can be considered a second order dynamics if a correct torque dispatching is operated.

Accordingly, the attitude dynamics control is designed in order to combine the following features:

1) The total angle of attack and aerodynamic roll dynamics are damped by making the roll and pitch torques a linear function of the angular rates, estimated by the attitude embedded model. The damping factor of the resulting oscillator is fixed at 1.
2) The yaw torque is calculated to drive the bank angle around the value requested by the CoM control law and to perform the BRMs. The value of the roll torque is adjusted to compensate of the aerodynamic roll dynamics.
3) The time derivative of the velocity angles affect in a know way the aerodynamic angles dynamics. The reference angular rates are adjusted to compensate for this effect.
4) The gyroscopic torques are estimated based on the nominal matrix of inertia and cancelled.

A typical evolution of some relevant signals of the attitude control is shown in Figure 14 and Figure 15.

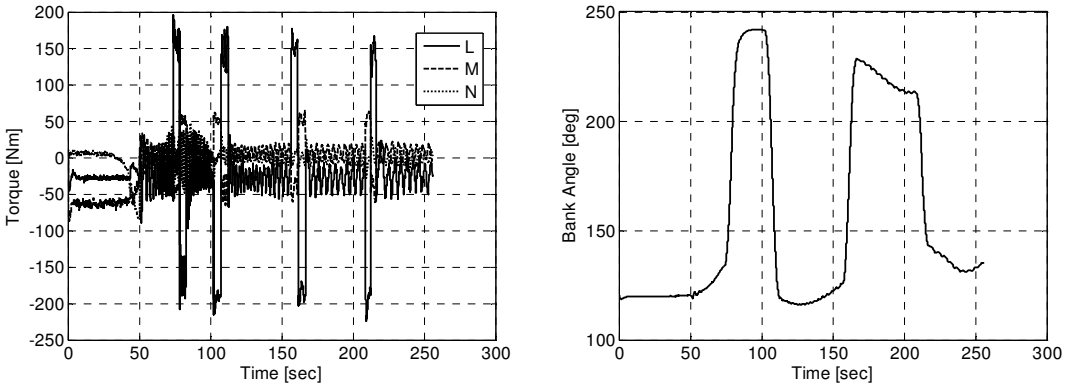

Figure 14. Commanded torque and bank angle.

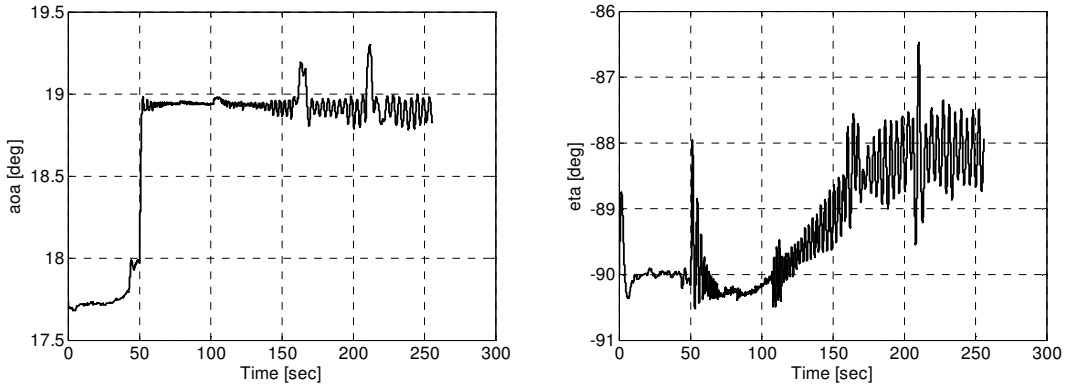

Figure 15. Total angle of attack and aerodynamic roll.

4. Montecarlo 6DOF preliminary results

A preliminary Montecarlo simulation campaign has been computed using a 6DOF simulator. Input variable randomization is the one listed on Table 2. In addition, the matrix of moments of inertia, the mass, and the thruster's dynamics (time-constants and delay) and orientation are also randomized.

The plots on Figure 16 and Figure 17 show the aerodynamic and atmospheric dispersions together with the resulting PDP dispersion. It has to be recalled that the PDP dispersion refers to the "navigated dispersion", this is, the error between the navigated states and the nominal mission PDP. Navigation errors will unavoidably combine to the ones shown below, since they cannot be handled by the control algorithm.

Another clarification that deserves to be pointed out is that the triggering algorithm plays a very important role on the shape and size of the PDP dispersion. In fact, two cases are included, at time-based triggering algorithm which assumes that the parachute is triggered based on the time calculated by the guidance algorithm, and a distance-based triggering algorithm in which the parachute is triggered when a local minima of the distance to the nominal PDP position is identified.

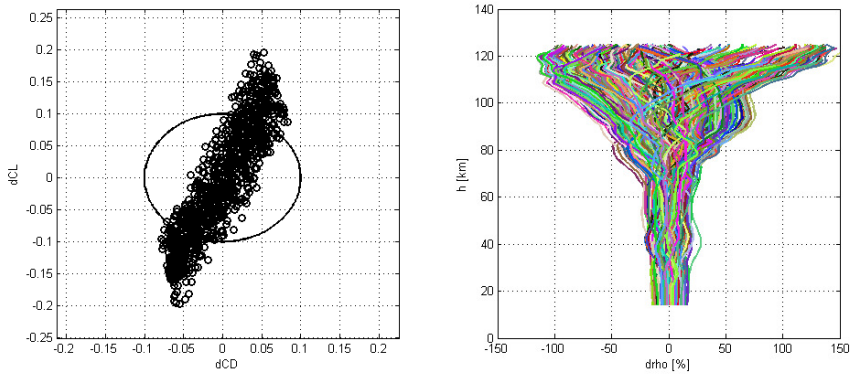

Figure 16. Aerodynamic and atmospheric dispersion. Circle on the left denotes 10 % aerodynamic coefficients dispersion.

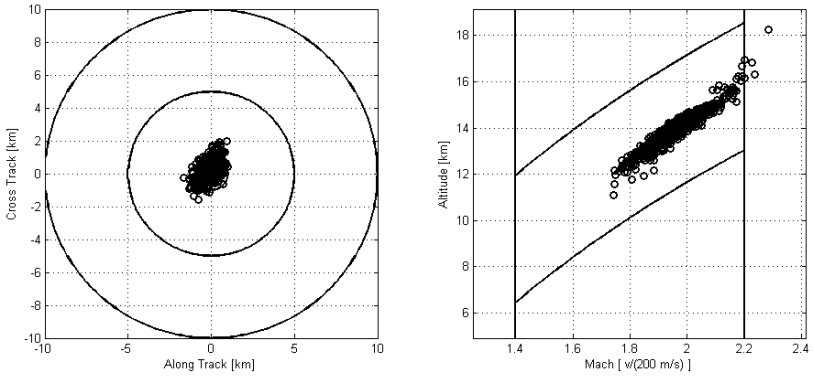

Figure 17. Dispersion at PDP using time-based triggering. Circles on the left denotes 1 km, 5 km and 10 km.

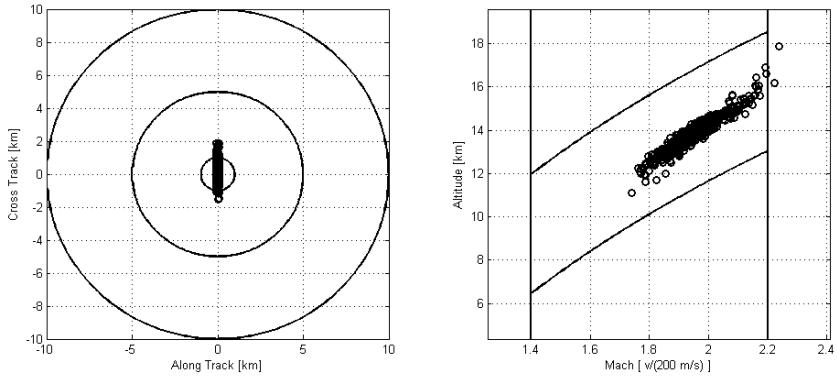

Figure 18. Dispersion at PDP using downrange-based triggering. Circles on the left denotes 1 km, 5 km and 10 km.

One outlier, on 300 tests, occurs in which parachute is triggered outside the safe parachute deployment conditions. Unfortunately, it has been observed that the altitude error is actually requested by the control unit in order to cancel (through the variation of the atmospheric density) the dispersion of the drag coefficient and the atmospheric density dispersion. In fact, downrange error on that test is only 300 m. Asking the altitude for following the guidance profile

or delaying parachute triggering would result on a large increase of the downrange error. Possible solutions to this rare case are currently being studied.

The dispersion of the navigated state at PDP shown in figures above is smaller than the one claimed by other approaches such as those presented in [4] and [8]. A direct comparison, however, would ask for ad-hoc analyses since, in general, the conditions of each algorithm do not exactly matches those considered of the other. For instance, a direct comparison would ask, at least, for similar 6DOF simulator and parachute triggering logic.

5. Conclusions

In this paper, the approach followed by Thales Alenia Space, in strict collaboration with the Politecnico di Torino, for the design of a guided entry algorithm has been described. As it has been shown, the selected approach, following the principles of the EMC methodology, is largely based on a detailed analysis and modelling of both the CoM and attitude dynamics. The result is a new model-based guided entry control scheme which differs from other approaches such as the Apollo-derived algorithms or recent path-planning techniques.

Preliminary simulations using a complex 6DOF simulator which includes the typical dispersion on entry conditions assumed for this kind of analysis shows promising results, which encourage further development and consolidation of the selected approach, together with a detailed performance and sensitivity characterization using a qualified Thales Alenia Space end-to-end simulator.

6. Acknowledgments

The authors would like to thank Paolo Martella and Stefano Portigliotti for their support and their inspiring work performed on EXOMARS.

References

[1] C. Cassi, A. Anselmi, V. Giorgio and G. Gianfiglio. 2010. ExoMars 2016 Mission Design Status. 61th International Astronautical Congress (IAC 2010).

[2] Paul B. Brugarolas, A. Miguel San Martin and Edward C. Wong. 2010. The RCS Attitude Controller for the Exo-atmospheric and guided entry phases of the Mars Science Laboratory. PhD Thesis. International Planetary Probe Workshop (IPPW-7).

[3] Kluever C. A.. Entry guidance performance for mars precision landing. Journal of Guidance, Control and Dynamics, Vol 31, No 6, 2008.

[4] Pigné, G., Clar, P., Ferreira, E., Bouaziz, L., & Caullaud, J. Navigation Guidance and Control of the Atmospheric Re-entry Demonstrator. Spacecraft Guidance, Navigation and Control Systems, Proceedings of the 3rd ESA International Conference held 26-29 November, 1996 at ESTEC, Noordwijk, the Netherlands.

[5] Carman, G. L., Ives, D. G., and Geller, D. K., “Apollo-Derived Mars Precision Lander Guidance,” AIAA Paper 98-4570, Aug. 1998.

[6] Tu, K.-Y., Munir, M. S., Mease, K. D., and Bayard, D. S., “Drag-Based Predictive Tracking Guidance for Mars Precision Landing,” Journal of Guidance, Control, and Dynamics, Vol. 23, No. 4, 2000, pp. 620–628.

[7] Bayard, D. Lu, W. Guidance and Control for Mars Atmospheric Entry: Adaptivity and Robustness 14th IFAC Congress Beijing, China 1999.

[8] Kron, A., de Lafontaine, J.. Control of mars guided entry (part II): Robust nonlinear dynamics inversion. 17th IFAC Symposium on Automatic Control in Aerospace (2007).

[9] Canuto E., Embedded Model Control: outline of the theory, ISA TRANSACTIONS, 2007, Vol. 46 (3), pag. 363-377, ISSN: 0019-0578, DOI: 10.1016/j.isatra.2007.01.006.

[10] Canuto E., Molano-Jimenez A, Massotti L, Drag-free control of the GOCE satellite: noise and observer design, IEEE transactions on control systems technology, pp. 9, 2010, Vol. 18, pag. 501 - 509, ISSN: 1063-6536, DOI: 10.1109/TCST.2009.2020169.

[11] Canuto E., Molano Jimenez A., C. Perez Montenegro, L. Massotti long-distance, drag-free, low-thrust, leo formation control for earth gravity monitoring, Acta Astronautica, 2011, in press

[12] Canuto E., Massotti L, Local orbital frame predictor for LEO drag-free satellites, ACTA ASTRONAUTICA, pp. 9, 2010, Vol. 66, pag 446 - 454,

[13] Canuto E., Massotti L, All-propulsion design of the drag-free and attitude control of the European satellite GOCE, ACTA ASTRONAUTICA, pp. 20, 2009, Vol. 64, pag 325 - 344,

[14] Canuto E., Drag-free and attitude control for the GOCE satellite, AUTOMATICA, 2008, Vol. 44 (7), pag 1766 - 1780,

[15] P. Martella, M. Buonocore, E. Canuto, A. Molano, R. Drai, L. Lorenzoni. 2011. Gnc design and performance of the exomars edl demonstrator. Presented at the 8th International ESA Conference on Guidance, Navigation & Control Systems, Karlovy Vary, Czech Republic, June 2011

[16] Philip C. Knocke, Prasun N. Desai, Timothy J. Parker et alii. 2004. Mars Exploration Rovers Landing Dispersion Analysis. AIAA/AAS Astrodynamics Specialist Conference and Exhibit, AIAA 2004-5093

[17] Robert D. Braun, Robert M. Manning. 2006. Mars Exploration Entry, Descent and Landing Challenges, Aerospace Conference, 2006 IEEE

[18] Adam Steltzner et alii. 2006. Mars Science Laboratory Entry, Descent, and Landing System. IEEEAC paper #1497

[19] ESA website. 26 January 2011. Mars Robotic Exploration Preparation Programme (MREP). http://www.esa.int/SPECIALS/Technology/SEMBC6WPXPF_0.html

[20] Richard Mattingly. 2010. Proposed MSR Campaign Description, available on: ftp://www.rssd.esa.int/pub/SRE-ITTs/documents/ITT(2010)-MSR Orbiter/RD/RD/MSR/

[21] Mendeck, G.F. and Carman, 2002. G.L. Guidance Design for Mars Smart Landers Using The Entry Terminal Point Controller. AIAA 2002-4502. AIAA Atmospheric Flight Mechanics Conference and Exhibit, Monterey.

[22] Jarret M. Lafleur and Chris J. Cerimele. 2008. Mars Entry Bank Profile Design for Terminal State Optimization. AIAA 2008-6213. AIAA Atmospheric Flight Mechanics Conference and Exhibit, Honolulu, Hawaii.

[23] Michael J. Grant, Ian G. Clarky, and Robert D. Braunz . 2010. Rapid Entry Corridor Trajectory Optimization forConceptual Design. AIAA 2010-7810. AIAA Guidance, Navigation, and Control Conference, Toronto, Ontario Canada.